Macromolecules
ARTICLE

Macromolecules **2009**, *42*, 8423–8434 **8423**
DOI: 10.1021/ma901631x

Effective Interactions and Self-Assembly of Hybrid Polymer Grafted Nanoparticles in a Homopolymer Matrix

Arthi Jayaraman[†] **and Kenneth S. Schweizer***[,‡]

[†]*Department of Chemical and Biological Engineering, University of Colorado, Boulder Colorado 80309, and* [‡]*Department of Materials Science and Engineering and Frederick Seitz Materials Research Laboratory University of Illinois, 1304 West Green Street, Urbana, Illinois 61801*

Received July 23, 2009; Revised Manuscript Received September 30, 2009

ABSTRACT: We apply the microscopic polymer reference interaction site model integral equation theory to study the structure and phase behavior of spherical nanoparticles with six symmetrically grafted chains in a homopolymer matrix that is chemically identical to the grafted polymer. Calculations of the particle−particle potential of mean force (PMF), pair correlation functions, and collective structure factors under athermal conditions and in the presence interfiller attractions are presented. Polymer grafted nanoparticles disperse or aggregate in the homopolymer matrix depending on how much of the filler surface is effectively covered by the tethered chains which sterically shield direct intercore attractions. If the nanoparticle volume is less than its total tether analogue, the filler surface is well shielded and nanoparticles tend to disperse. For smaller filler cores (∼2 nm) the grafting density is more brush-like, and the PMF becomes more attractive at contact with increasing matrix chain length due to decreasing wettability of the tether layer. For larger particles with much lower grafting density, the effect of matrix chain length on the PMF is different, and for all matrix lengths, the PMF at contact can be switched from attractive to repulsive by increasing the grafted chain length. At nonzero filler concentrations, nanoparticles with tether volume matching the filler core volume exhibit a critical attraction strength below which repulsive forces dominate resulting in good dispersion. Above the critical attraction strength, enthalpic effects dominate and the PMF becomes increasing attractive at contact and favors nanoparticle aggregation. When the tether and matrix chain lengths are equal, as the nanoparticle size increases less of its surface is shielded and modest clustering occurs due to direct core−core attraction and matrix-induced depletion attraction. The microphase spinodal temperature of nanoparticles with six grafted chains monotonically decreases upon homopolymer addition ("dilution" behavior), while nanoparticles with only one or two grafted chains exhibit subtle competition between dilution and matrix-mediated depletion attraction that increases their microphase separation temperature.

I. Introduction

Polymer nanocomposites,[1−3] composed of nanoparticle additives ("fillers") in a polymer matrix, offer a variety of enhanced thermal, mechanical, optical, and electronic properties relative to pure polymeric materials due to interactions between fillers and the matrix. A major challenge is the rational control of the spatial organization of nanoparticles in a polymer melt. Over the past few years, several research groups have functionalized nanoparticle surfaces with ligands in an effort to control their dispersion or self-assembly in a homopolymer or block copolymer matrix.[4−15] For example, if nanoparticles are grafted with chains compatible with the matrix polymer, filler dispersion is possible to realize.[16] Most work has focused on spherical particles functionalized with chemically attached chains at high surface grafting density.[15−17] Under these brush-like conditions and at fixed polymer chemistry, when the molecular weight of matrix chains is lower (higher) than that of grafted polymer the nanoparticles disperse (aggregate). This is because it is entropically favorable for the shorter matrix chains to penetrate and wet the grafted polymer layer, thus leading to dispersion of the polymer grafted particles in the matrix.[18]

More recently, nanoparticles grafted with a relatively small and controlled number of synthetic chains,[19−22] such as single-tethered CdTe quantum dots,[20] gold nanoparticles with a single poly(ethylene oxide) tether,[23] and fullerenes end-capped with poly(methyl methacrylate),[24] have been synthesized. Theoretical studies[25−33] have shown that concentrated solutions and melts of this new class of lightly grafted hybrid nanoparticles (in the absence of a matrix) can self-assemble into a variety of microphase-separated nanostructures. In the presence of a matrix the potential of mean force (PMF) between two moderately grafted nanoparticles placed in a homopolymer matrix has been found to be repulsive even when the grafted polymers are much shorter than the polymer matrix.[34] This is unlike highly grafted particles in a homopolymer matrix, where the PMF is attractive if the grafted polymer is shorter than the matrix chain. The focus of this paper is to present a detailed theoretical study of such moderately grafted nanoparticles as fillers in a homopolymer matrix as a function of increasing nanoparticle concentration.

Recently[32,33,35] we generalized and applied the microscopic polymer reference interaction site model (PRISM) integral equation theory to study concentrated solutions and melts of one-, two- and four- tethered spherical nanoparticles, and lightly (one- and two-) tethered nanoparticles in a homopolymer melt. The role of tether length, particle size, number and placement of tethers, total packing fraction, and interparticle attraction strength on the real space statistical structure and scattering patterns, and tendency toward aggregation and/or microphase separation, was investigated. Strong concentration fluctuations indicative of clustering and/or incipient microphase ordering is

*Corresponding author. E-mail:kschweiz@illinois.edu.

Published on Web 10/19/2009

predicted with increasing total packing fraction and/or nanoparticle attraction strength. In analogy with block copolymers, a microphase spinodal curve was deduced by extrapolation to zero of the inverse intensity of the small angle scattering peak. For tethered nanoparticles with a core diameter twice that of the monomer, the microphase spinodal temperature grows roughly as a power law of packing fraction. The apparent scaling law exponent is less than unity and varies with the number of tethers, and the spinodal curve shifts to lower temperatures with increasing number of tethers. The microphase spinodal calculations for single-tethered particles were found to be in good agreement with a recent simulation study by Glotzer and co-workers.[29,30] Upon increasing the nanoparticle diameter, the microphase spinodal temperature decreases, and its packing fraction dependence qualitatively changes due to a competition between an increased tendency for macrophase separation and a decreased tether-mediated driving force for microphase ordering.

For single- and two-tethered spherical nanoparticles dissolved in a homopolymer melt of matched chemistry[35] the theory predicts a competition between tether-induced steric stabilization that can induce microphase ordering, and matrix-induced depletion-like attraction that can drive macrophase separation. For single-tethered nanoparticles the shape of the microphase spinodal curve is a combination of dilution-like (as in copolymer−homopolymer mixtures or solutions of diblock copolymers) and depletion-like (as seen in colloid−polymer mixtures) behavior. Furthermore, the microphase spinodal temperature is a nonmonotonic function of matrix chain length, and as the nanoparticle size is increased at a constant tether length the tendency for macrophase separation increases. As the nanoparticle size and tether length are both increased, keeping the total volume of tethered monomers equal to the volume of the nanoparticle, the shape of the microphase spinodal curve remains unchanged, but the effect of varying matrix polymer length on the spinodal temperature diminishes. As the number of tethers is increased, the microphase spinodal curves become more dilution-like and the effect of matrix polymer length, tether length, and particle size on the spinodal temperature is reduced.

In this paper, we present a detailed PRISM theory study of moderately grafted spherical nanoparticles that carry six tethers dissolved in a homopolymer melt. This work is partially motivated by the recent experiments of Kumar and co-workers[4] on polystyrene-grafted silica nanoparticles (∼14 nm diameter) dissolved in a polystyrene matrix, which discovered novel self-assembled structures attributed to a competition between graft-induced repulsion and direct nanoparticle attraction when the degree of grafting is modest. In addition, after our manuscript was submitted a molecular dynamics simulation study of dilute moderately grafted nanoparticles in a homopolymer matrix[34] was reported which is relevant to our theoretical results. Specifically, these simulations found that as a consequence of high nanoparticle curvature, a repulsive potential-of-mean force and filler dispersion can be achieved under athermal conditions, even if the tether chains are much shorter than the homopolymer matrix degree of polymerization if the grafting density is relatively low. This occurs despite the fact that the matrix chains do not penetrate to the particle surface. Interestingly, these conditions result in aggregation at higher grafting density and short grafted chains, suggesting that dispersion or clustering of fillers depends on how much nanoparticle surface is exposed to the homopolymer matrix which in turn is sensitive to grafted chain length. We also find via potential of mean force (PMF) calculations that under athermal and dilute filler conditions whether dispersion or aggregation of nanoparticles occurs depends mainly on how much of the filler surface is effectively covered by the grafted chains that sterically shields the direct intercore attraction. For example, nanoparticles with six tethers have an attractive PMF at contact if the tethers are short enough, but a repulsive PMF at contact for longer tethers. As the nanoparticle core diameter increases, at fixed number and length of tether chains, the potential of mean force at contact changes from repulsive to attractive since the grafted chains no longer efficiently cover the larger nanoparticle surface. Since the system of six-tethered nanoparticles of core diameter greater than a few nanometers is unlike dense brush coated filler, the effect of matrix length on the PMF is different from a purely repulsive form. In addition to the dilute filler limit, we also present calculations that address the effect of increasing filler concentration on the pair correlation functions and structure factors for varying nanoparticle size, tether length, matrix chain length, and particle−particle attraction strength. Microphase spinodal curves are determined and suggest a dilution-like behavior, unlike phase boundaries for more lightly grafted nanoparticles,[35] which exhibit subtle competition between dilution and depletion effects.

The paper is organized as follows. In section II the model, theory and parameters used in this study are discussed. In section III, calculations of the homopolymer matrix induced effective interactions and particle−particle pair correlations in the dilute filler limit, under both athermal conditions and with filler attractions, are presented. The PMF, filler pair correlation functions, collective structure factors, and extrapolated microphase spinodal boundaries for finite concentrations of tethered nanoparticles are studied in section IV. The paper concludes with a summary and brief discussion in section V.

II. Model and Theory

A. Model and Interaction Potentials. Figure 1 presents a schematic of spherical nanoparticles with six flexible chain tethers symmetrically and permanently grafted on a filler of diameter D in a homopolymer matrix. The tether and matrix polymer are treated as freely jointed chains (FJC) of N_p and N_m spherical interaction sites (monomers), respectively. The coarse grained monomer or segment has a diameter d which is the unit of length used throughout the paper. Monomers are connected by a rigid bond (persistence length for a FJC) length $l = 1.4d$, which is a typical persistence length of flexible synthetic polymers,[36] and is also the characteristic value of the classic Kremer-Grest bead−spring simulation model.[37,38] The absolute value of d is, of course, not uniquely defined for a FJC model. It can be estimated based on equating the persistence length of a real chain to that of the FJC: $1.4d = (C_\infty + 1)l_b/2$, where l_b is a backbone chemical bond length (∼0.15 nm) and C_∞ is the characteristic ratio. On the basis of this mapping, $d \sim 0.6$ nm for polystyrene or polymethymethacrylate. Of course, other mappings of real monomers onto FJC segments will lead to different estimates of d. For example, a value of $d \sim 1$ nm will be obtained if one requires the volume of a segment equals the space-filling volume of 2−3 (of the order of a persistence length) real polystyrene monomers. Hence, for semiquantitative purposes we view the length scale d as being on the order of a nanometer. We use the subscripts "p", "c", and "m" to denote tether polymer, nanoparticle, and matrix polymer, respectively. The total mixture packing fraction is defined by η, and the fraction of η composed of polymer-tethered particles is the composition variable, ϕ.

The site−site pair decomposable interactions between tether monomers, U_{pp}, tether monomers and nanoparticles, U_{pc}, matrix monomers, U_{mm}, matrix and tether monomers, U_{mp}, and matrix monomer and nanoparticles, U_{mc}, all include a hard core repulsion. The only attractive interactions present are between nanoparticle cores, U_{cc}, modeled beyond contact as the attractive branch of the colloid

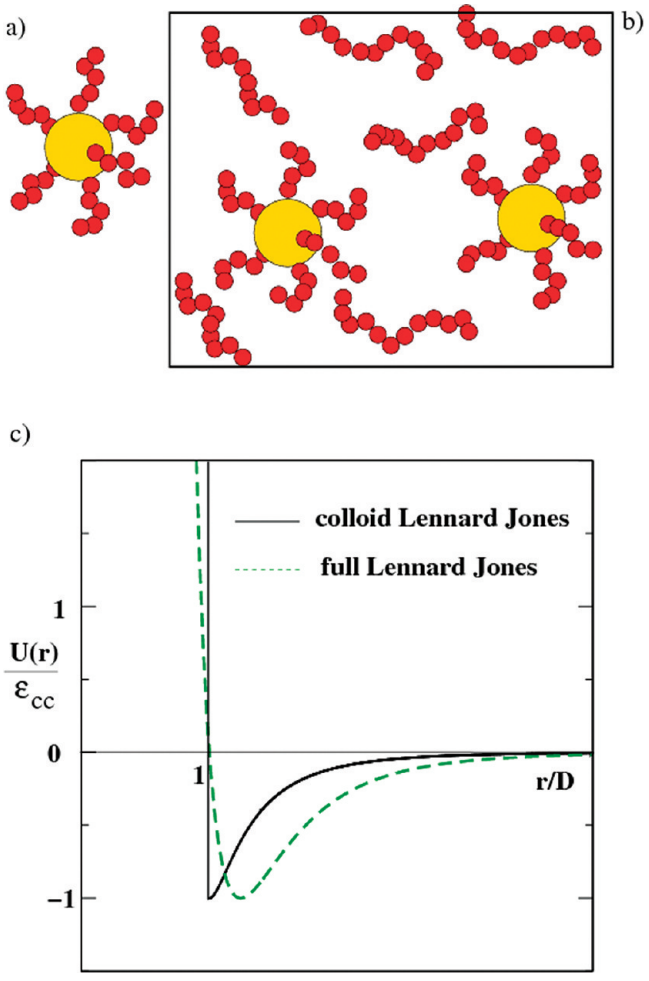

Figure 1. Schematic of (a) six-tethered nanoparticle, (b) six-tethered nanoparticle in a homopolymer matrix, and (c) the colloid LJ potential.

Lennard-Jones (CLJ) potential.[39] The latter describes the interaction between two nanospheres as a pairwise sum over LJ potentials between elementary units of size b. An example of the attractive branch of the CLJ potential for a particle with $D = 2b$, where $b = d$, is shown in Figure 1; its strength is characterized by the value at contact, $-\varepsilon_{cc}$.

Our model system is meant to mimic a polymer nanocomposite composed of grafted nanoparticles dissolved in a homopolymer melt, where the matrix and grafted chains are of the *same* chemistry, nanoparticle-homopolymer and homopolymer-homopolymer attractions are weak and very similar, and nanoparticles have a different chemistry from the polymer chains resulting in unbalanced van der Waals attractions of variable strength.

B. Polymer Reference Interaction Site Model Theory. PRISM is an equilibrium theory that describes well the structure of both suspensions and dense melts composed of hard spherical particles and linear chains.[32,40−43] The theory is based on the matrix Ornstein−Zernike-like or Chandler-Andersen integral equations[44] that relate the total site−site intermolecular pair correlation function between different sites, $h_{ij}(r) = g_{ij}(r) - 1$, to the site−site intermolecular direct correlation function, $C_{ij}(r)$, and intramolecular probability distribution functions, $\omega_{ij}(r)$. The matrix PRISM equations in Fourier space are

$$\mathbf{H}(k) = \Omega(k)\mathbf{C}(k)[\Omega(k) + \mathbf{H}(k)] \quad (1)$$

$$H_{ij}(k) = \rho_i \rho_j h_{ij}(k) \quad (2a)$$

$$\Omega_{ij}(k) = \rho \sum_{\alpha=1}^{N_i} \sum_{\beta=1}^{N_j} \omega_{\alpha i \beta j}(k) \quad (2b)$$

Here, N_i is the number of interaction sites of type i, ρ_i the total site density of species i, and ρ the molecular number density. The 3×3 matrices $\mathbf{H}(k)$, $\mathbf{C}(k)$, and $\mathbf{\Omega}(k)$ describe correlations of three types of sites, "c", "p", and "m"; the site inequivalency associated with chain end and junction effects are ignored (preaveraged) as in prior applications of PRISM theory to homopolymers,[36,45] polymer nanocomposites,[40−43] and block copolymers.[46,47] Explicit equations for $h_{ij}(k)$, the tethered nanoparticle $\omega_{ij}(k)$, and the partial collective structure factors, $S_{ij}(k)$, are given in ref 35.

Possible nonideal conformational perturbations of the tether and matrix polymers are not taken into account. In principle, they can be treated using the fully self-consistent and computationally intensive version of PRISM theory, which involves a medium-induced solvation potential and solution of an effective single-chain problem via Monte Carlo simulation.[36,48] However, the construction and testing of such a solvation potential for grafted particles in a polymer melt is presently an unsolved problem in the framework of PRISM theory. Moreover, we expect chain stretching or contraction effects to be most important in dilute solutions, when particle-polymer or polymer−polymer interactions are attractive, and/or if the tether grafting density is high. Our focus is melt-like packing fractions, moderate grafted nanoparticles, with polymer-related attractions absent, conditions for which conformational nonidealities of excluded volume and enthalpic origin are expected to be minimized. In addition, we do not consider very long tethers, which should also mitigate large nonideal conformational effects, and minimize unphysical intrachain overlaps present in any ideal chain model.[36]

Approximate closure relations are required to solve the PRISM equations. For polymer nanocomposites (PNC) the site−site Percus−Yevick (PY) closure[36,40,43−45] is quite accurate for all direct correlation functions except particle−particle. Previous PNC studies employed the hypernetted chain (HNC) approximation[40] for the latter, which also ensures the physical condition $g_{cc}(r) > 0$ holds for all r. If σ_{ij} is the distance of closest approach between sites of type i and j, the hard core impenetrability conditions are as follows:

$$g_{ij}(r) \equiv 0, \mathrm{r} < \sigma_{ij} \quad (3)$$

Outside the hard core the site−site PY approximation[36,40,44,45] is employed for all, except particle−particle, direct correlations:

$$C_{ij}(r) = (1 - e^{\beta U_{ij}(r)}) g_{ij}(r), \quad r > \sigma_{ij} \quad (4)$$

and the HNC closure is adopted for the particle−particle direct correlation function:

$$C_{cc}(r) = h_{cc}(r) - \ln g_{cc}(r) - \beta U_{cc}(r), \quad r > \sigma_{ij} \quad (5)$$

Our prior work for the single tether nanoparticle system demonstrated quite good agreement with simulation,[29] which supports the usefulness of these atomic closures. For polymer blends and block copolymers composed of monomers of (nearly) the same size the so-called "molecular closures"[36] are generally the most accurate. Whether such closures are

better for polymer nanocomposites with hybrid nanoparticles remains to be explored.

To efficiently solve the six coupled nonlinear integral equations we employ the Kinsol algorithm[49] which employs the inexact Newton's method and has a relatively high ease of convergence for complex nonlinear integral equations, especially compared to Picard algorithm. Solution of the PRISM equations yields the pair correlation functions, $g_{ij}(r)$, and partial collective structure factors, $S_{ij}(k)$.

C. System Parameters. There are many controllable material parameters: tether degree of polymerization, N_p, number of tethers, f, placement of tethers, ratio of particle-to-monomer diameter, D/d, matrix polymer degree of polymerization, N_m, total fluid packing fraction, η, volumetric composition of tethered particles, ϕ, and interparticle attraction strength in units of the thermal energy, ε_{cc}. Most calculations are performed for six symmetrically placed tethered particles with $N_p = 8$, 18, 27, and 50, $D/d = 2$, 3, and 6, and polymer matrix lengths ranging from $N_m = 1$ ("solvent") to 50. The effect of variable tether placement in the absence of free homopolymer has been previously studied.[33] The attraction strength ε_{cc} is varied from 0 (athermal) to several kT. The total packing fraction, η, is varied from 0.4 to 0.5, representative of a dense melt.

D. Grafting Density. A measure of the surface grafting density is computed by dividing the number of tethers by the nanoparticle surface area. The units of the surface grafting density is taken to be the number of chains per unit monomer surface area (d^2), which for particles of size $D/d = 2$, 3, and 6 with six grafted chains yields 0.48, 0.21, 0.05 chains/d^2, respectively.

III. Dilute Filler Limit

Earlier work on polymer nanocomposites[42,43,50] with bare nanofillers has shown that the homopolymer melt induces a strong and spatially short-range (monomer scale) depletion attraction causing macrophase separation of the nanofillers. Prior simulation[29] and theoretical work[31−33] has demonstrated that microphase separation can occur for dense solutions of lightly tethered nanoparticles. For the case of lightly tethered particles in a polymer matrix, there are potentially three qualitatively different organizational scenarios that can arise due to the competition between interparticle attractions, steric repulsion between grafted tethers, and filler-homopolymer matrix mixing considerations including the depletion-like entropic attraction. (i) Strong intertether repulsions can sterically shield direct nanoparticle attractions, and if the depletion effects are weak, then the fillers can form a well-dispersed correlated fluid in the homopolymer matrix. (ii) If the intertether repulsion is weak, and nanoparticle attractions are strong enough, then the interparticle attraction plus matrix-induced depletion effects can result in macroscopic phase separation into matrix polymer rich and nanoparticle rich coexisting phases. (iii) If interparticle attractions are strong enough, and sufficient steric stabilization exists due to tether repulsion to preclude macrophase demixing, then stable aggregate formation and/or microphase type of ordering can occur. The competing physical effects that determine the thermodynamics and structure are functions of chemistry (via nanoparticle attraction strength), tether grafting density, tether chain length, matrix chain length, total packing fraction, and mixture composition.

In this section we present calculations of the filler PMF at infinite dilution in a homopolymer matrix at $\eta = 0.4$. The influence of absolute and relative tether and matrix degrees of polymerization, nanoparticle core diameter, and direct filler attraction strength are investigated. Throughout the paper we focus exclusively on the nanoparticle-nanoparticle pair correlations and collective structure factors.

A. Athermal Limit. We first consider the purely entropic athermal limit. Figure 2 presents nanoparticle pair correlation functions, $g_{cc}(r)$, and the corresponding potential of mean force (PMF), $W_{cc}(r)$, for $D/d = 2$ (top panel), 3 (middle panel), and 6 (bottom panel) for fixed tether length $N_p = 8$ and variable matrix length N_m. For $N_p = 8$ and $D/d = 2$, the total space filling volume of each tether ($N_p\pi d^3/6$) equals the volume of the nanoparticle; for $D/d = 3$ ($D/d = 6$) the nanoparticle volume is slightly (much) greater than that of one tether. By knowing the total volume of the monomers in each tether one can estimate how much space these monomers occupy above the nanoparticle surface. The volume of the monomers is more relevant than their surface area because it is tethered monomer crowding and their excluded volume interactions that dictate if another particle or a matrix monomer can penetrate the grafted layer.

For $D/d = 2$ (Figure 2a) and $N_m = 1$ (good solvent limit), one sees a local correlation hole ($g_{cc}(r) < 1$) over all interparticle separations up to $r \sim 3.5D$, beyond which the bulk value of unity is achieved. This behavior arises from the steric hindrance associated with the grafted tethers, which shields the nanoparticle surface and prevents contact of filler surfaces. As the matrix polymer length, N_m, increases to 8 and then 50, $g_{cc}(r)$ approaches the bulk value at increasingly shorter interparticle distances. This trend is consistent with the idea that at fixed grafted tether length, as the matrix polymer length increases the homopolymer matrix chains are increasingly expelled from the grafted tether layer resulting in fillers being more pushed together. The corresponding PMF (Figure 2b) shows the effective repulsion at contact does not vary much with matrix polymer length, but as the latter increases ($N_m = 50$), a very weak attraction emerges at an intermediate filler separation ($\sim r/D = 2.5$). This agrees with the molecular dynamics PMF results of Smith and Bedrov[34] for particles of size $D = 5$ nm grafted with polymers of length $N = 10$ in a matrix of length 70 which has a nearly the same grafting density as our $D/d = 2$, $N_p = 8$ system. In contrast, at much higher brush-like grafting density the potential of mean force would have a stronger midrange attraction as found by Smith and Bedrov[34] at a grafting density of 0.8 chains/nm^2, and in the Monte Carlo simulations and density fuctional theory (DFT) studies of Striolo and Egorov.[51] In the latter DFT study, the potential of mean force between two homopolymer grafted nanoparticles in homopolymer solution with athermal interactions exhibited repulsion at contact and a midrange attraction. The latter arises between the two particles if the length of the matrix polymer exceeds that of the grafted homopolymers. However, it is important to note that their homopolymer matrix concentration was low and not representative of a melt.

Results for $D/d = 3$ are shown in Figure 2, parts c and d for $N_m = 4$, 8, and 25. In strong contrast to the local correlation hole found when $D/d = 2$, here $g_{cc}(r/D = 1) > 1$, implying that the nanoparticle surfaces can come into contact and local liquid-like ordering is possible. This occurs since at $D/d = 3$ the grafting density is significantly lower than for $D/d = 2$, and tethers of length $N_p = 8$ are too short to effectively cover the nanoparticle surface. As the matrix polymer length increases, $g_{cc}(r)$ at contact decreases, but increases at $r \sim 1.15D$. For the shortest matrix polymer ($N_m = 4$), the PMF in Figure 2d is more attractive at contact, and more repulsive in the barrier region than the larger matrix lengths ($N_m > 4$). These trends are sensitive to tether length, as shown in Figure 3.

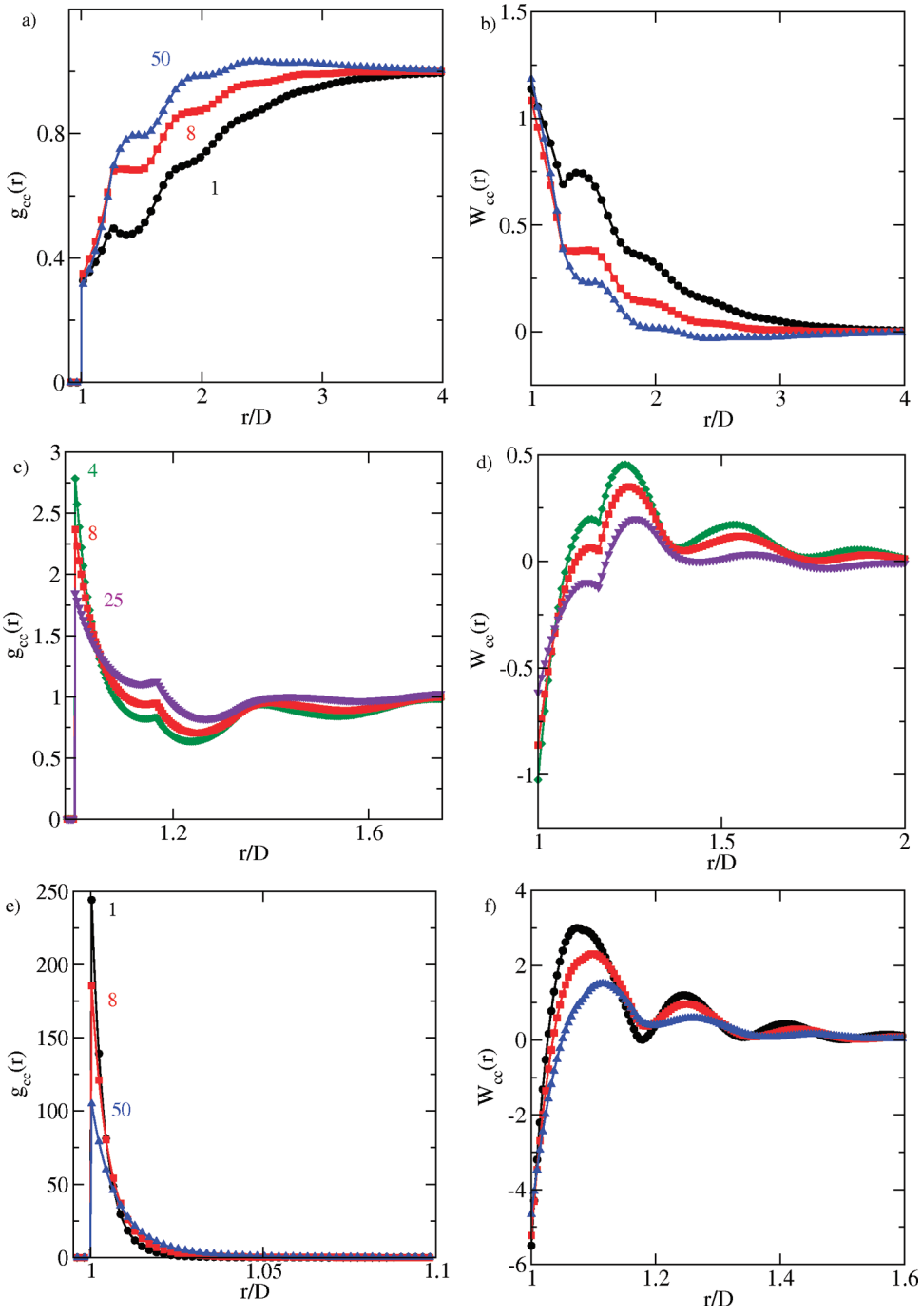

Figure 2. Dilute limit particle−particle pair correlation function, $g_{cc}(r)$, and potential of mean force, $W_{cc}(r)$, for nanoparticle size $D/d = 2$ (a and b), $D/d = 3$ (c and d), and $D/d = 6$ (e and f), tether length $N_p = 8$ and varying matrix length $N_m = 1$ (circle), 8 (square), 25 (downward triangle), 50 (upward triangle), at $\eta = 0.4$ under athermal conditions.

For the largest $D/d = 6$ filler (Figure 2, parts e and f), the tethers are too short to induce steric stabilization, and the PMF is similar to that of a bare nanoparticle in a homopolymer matrix where enormous contact depletion attractions exist.[40] More generally, note that the trends observed for $D/d = 3$ and 6 are the opposite of what is seen for large particles (or flat surfaces) at high grafting density.[16,51] For the latter systems, increasing matrix polymer length leads to increasing attraction between the particles, an effect associated with reduced wettability or interpenetration of matrix chains in the grafted layer as N_m becomes large compared to N_p. Clearly, a particle of size $D/d = 3$ or 6 with six grafted polymers of length $N_p = 8$ is not well described as a flat brush layer. More generally, the behavior of the $D/d = 3$ and 6 systems is likely relevant to the regime of moderate grafting density of nanofillers dissolved in chemically matched homopolymer melts.[4]

We now explore the question of whether the PMF between the nanoparticles can be switched from attractive to repulsive by increasing the grafted polymer length, and if so what is the role of the matrix chain length. Figure 3 presents calculations of $g_{cc}(r)$ and the PMF at a higher tether length for $D/d = 3$ and 6. For the $D/d = 3$ system (Figure 3, parts a and b), we choose $N_p = 27$ to ensure that the total space filling volume of the tether equals the nanoparticle volume, allowing for a fair comparison with the $D/d = 2$ and

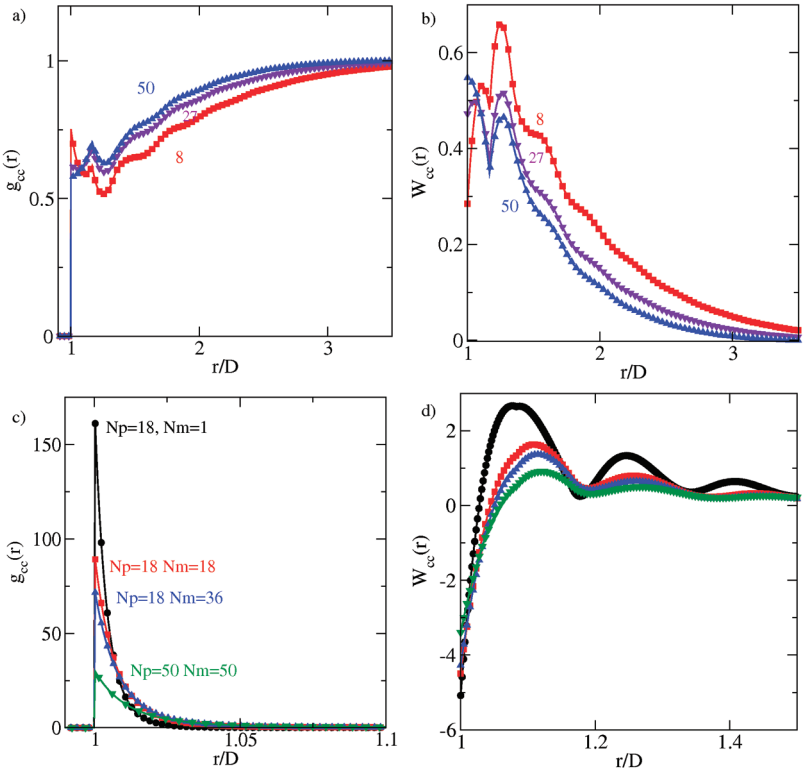

Figure 3. Dilute limit particle−particle pair correlation function, $g_{cc}(r)$, and potential of mean force, $W_{cc}(r)$, for $D/d = 3$, $N_p = 27$ (a and b), and $D/d = 6$, $N_p = 18$ and $N_p = 50$ (c and d), at varying matrix lengths, $N_m = 1$ (circle), 8 (square), 25 (downward triangle), 50 (upward triangle), at $\eta = 0.4$ under athermal conditions.

$N_p = 8$ system. For $D/d = 3$ and $N_p = 27$, a correlation hole in g_{cc}(r) occurs for all matrix chain lengths (Figure 3a), the depth and spatial range of which increases with decreasing matrix degree of polymerization, trends similar to the $D/d = 2$ and $N_p = 8$ system (Figure 2a) which is also seen in Figure 3b. Unlike the $D/d = 2$ system (Figures 2a and 2b), when $D/d = 3$ the PMF at contact is more sensitive to matrix chain length, increasing slightly with N_m. The key point is that by increasing the grafted polymer length, the filler PMF at contact can be switched from attractive (Figure 2d) to repulsive (Figure 3b) for all matrix chain lengths. This again confirms that the ratio of the tether to nanoparticle core volume is a critical parameter, which can alter the behavior of hybrid fillers from aggregated to dispersed.

Analogous calculations for $D/d = 6$ are shown in Figure 3, parts c and d. As the tether length increases from $N_p = 18$ to 50, $g_{cc}(r)$ at contact dramatically decreases by a factor of 6. Unfortunately, we could not obtain a converged numerical solution of the PRISM equations for high tether lengths, but based on the above trends for $D/d = 3$ and 6 we are confident that as the tether length is increased to $N_p = 256$, if the total volume of the tether and particle core are equal then the effective interaction between the $D/d = 6$ fillers will again be repulsive.

B. Effect of nanoparticle-nanoparticle attractions. We now study the consequences of direct filler−filler core attraction. Figure 4 presents PMF calculations for varying D/d and N_p with $N_m = N_p$ at high nanoparticle attraction strengths of $5kT$ and $10kT$. For comparison, a PMF computed based on simply adding the $W_{cc}(r)$ under athermal conditions and the bare potential $U_{cc}(r)$ is also shown (dashed curves). The latter is *approximate* since it ignores many body effects associated with the fact that beyond the infinite dilution limit the consequences of grafted chains and direct core attractions on the filler PMF are neither additive nor independent.

For $D/d = 2$ (Figure 4a) and tether length $N_p = 8$, the correctly computed PMFs (solid curves) are attractive at contact, in contrast to the repulsive $W_{cc}(r)$ for the same system under athermal conditions (Figure 2a). The large direct interparticle attraction allows a gain in enthalpy via particle contact which can overcome the grafted tether repulsions. As the direct attraction strength increases the PMF at contact deepens and the repulsive barrier intensifies. The dashed curves in Figure 4a are the approximate additive analogues. The neglect of many body effects results in a much stronger contact attraction and the complete absence of a repulsive barrier.

Figure 4b shows the PMF for $D/d = 3$ with six tethers of length $N_p = 8$ and 27 at $\varepsilon_{cc} = 5kT$ and $10kT$. The trends for $D/d = 3$ and $N_p = 8$ are similar to that seen for $D/d = 2$ and $N_p = 8$, with the effective attraction at contact and repulsion at further distances, both more intense for the larger nanoparticle. As the tether length increases from 8 to 27, there is little change of $W_{cc}(r)$ at contact, but a much longer range repulsive tail emerges at the same particle−particle attraction strength, which is even stronger at $\varepsilon_{cc} = 10kT$ compared to $5kT$. As for the $D/d = 2$ system, the approximate additive PMF analogues miss key features thereby demonstrating the presence of strong nonadditivity of the direct and polymer-mediated interactions.

For $D/d = 6$ (Figure 4c) and tether length $N_p = 8$, very strong attractions at contact are present and oscillations of the repulsive part of the PMF occur at larger filler separations. These oscillations disappear, and a long-range repulsive tail emerges, as N_p grows from 8 to 50. The longer range repulsive tail arises from repulsive interactions between the grafted chains which are enhanced in range and intensity as

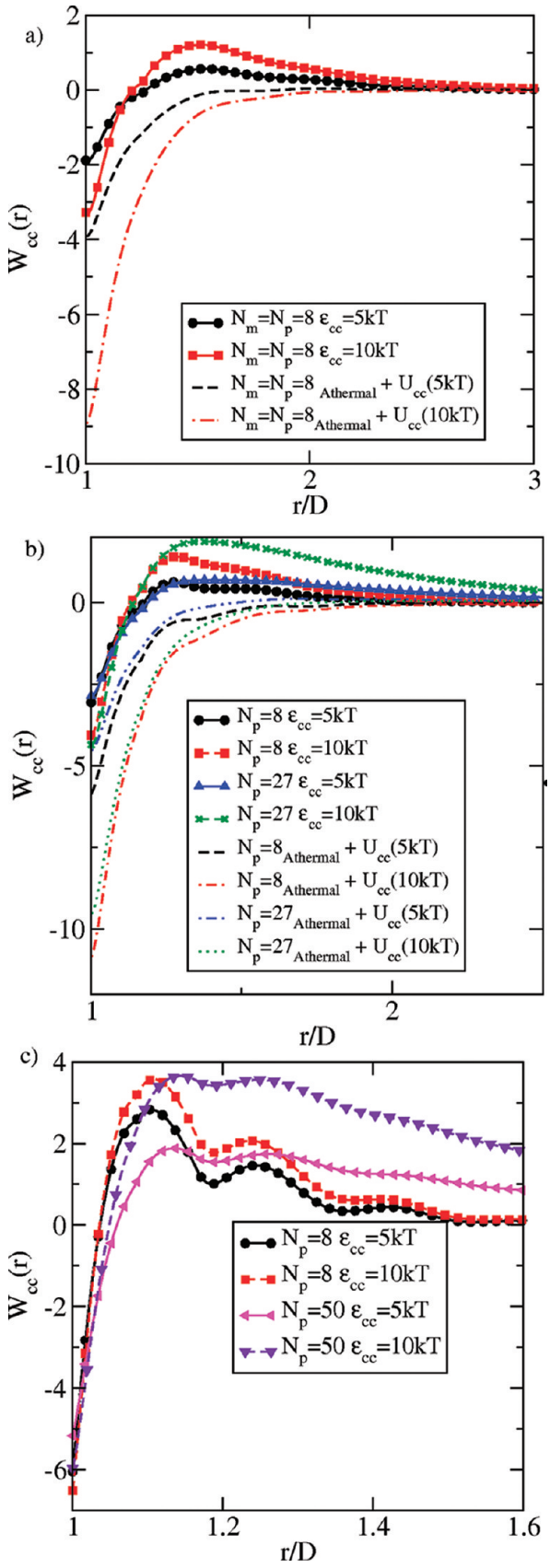

Figure 4. Dilute limit potential of mean force for (a) $D/d = 2$, $N_p = 8$, (b) $D/d = 3$, $N_p = 8$ and 27, (c) $D/d = 6$, $N_p = 8$ and 50, at fixed $N_m = N_p$ and $\eta = 0.4$ for direct filler−filler attraction strengths of $5kT$ and $10kT$. The dashed curves with no symbols are the approximate additive analogues.

the tether N_p grows. For $N_p = 50$, as the direct interparticle attraction strength increases, closer particle−particle contacts occur resulting in a stronger repulsive barrier at intermediate interparticle separations.

IV. Structure and Phase Behavior with Increasing Filler Concentration

We now consider a selection of the same systems examined in section III as a function of filler composition from $\phi = 0$ (dilute nanoparticle limit) to 1 (pure filler fluid) at a melt-like total mixture packing fraction of $\eta = 0.4$ or 0.5. For simplicity, the tether and matrix polymer chain lengths are constrained to be equal in the first two subsections.

A. Athermal conditions. Figure 5 presents the PMF and pair correlation under athermal conditions at $\eta = 0.4$ for $\phi = 0.2$, 0.5, and 0.8. Both D/d and tether length, N_p, are varied at fixed matrix polymer length $N_m = N_p$. For the smallest nanoparticles ($D/d = 2$, Figure 5a), increasing filler loading only weakly modifies the PMF and $g_{cc}(r)$ relative to the infinitely dilute result ($\phi -> 0$) in Figure 2b. The physical reason is the grafted chains crowd the surface of the particle and steric hindrance plays the dominant role. This is not the case for the $D/d = 3$ and $N_p = N_m = 8$ system shown in Figure 5b. At $\phi = 0.2$, the PMF at contact is attractive at contact and weakly repulsive for $r/D \sim 1.25$. At these low compositions the steric induced repulsion and the matrix-induced depletion attraction compete. As ϕ increases from 0.2 to 0.5, the PMF at contact becomes less attractive and develops two repulsive peaks in the region $1 < r/D < 1.5$ due to increased intermolecular crowding of the particles, and this enhanced steric hindrance begins to overcome the matrix-induced depletion attraction. As ϕ increases to 0.8, the PMF becomes repulsive at contact and has a weaker repulsive barrier. At this composition the steric stabilizing effects of the grafted polymers is dominant and favors dispersion of the nanoparticles.

As the tether length increases to $N_p = N_m = 27$ (Figure 5c), trends similar to the $D/d = 2$ and $N_p = N_m = 8$ system are predicted, with $W_{cc}(r)$ being systematically lower for $D/d = 3$. This is likely because for fixed D/d , the lower tether length $N_p = 8$ does not cover the particle surface as much as when $N_p = 27$. One way to quantify how well the surface is covered is to choose tethers whose total additive monomer volume matches the total particle volume. When this condition is satisfied the systems appear to behave in a similar fashion as seen by comparing the results for $D/d = 2$ and $N_p = 8$ with their $D/d = 3$ and $N_p = 27$ analogue.

B. Effect of nanoparticle-nanoparticle attractions. Figure 6 presents the PMF, $g_{cc}(r)$, and collective filler structure factor, $S_{cc}(k)$, for $D/d = 2$ and 3, $N_p = N_m = 8$ and 27, at $\eta = 0.4$, for a mixture composition of $\phi = 0.2$ and increasing inter-filler attraction strengths, ε_{cc}. For $D/d = 2$ and $N_p = N_m = 8$ at $\varepsilon_{cc} = kT$ (Figure 6a), $W_{cc}(r)$ is weakly repulsive at contact, becomes slightly more repulsive up to r/D = 1.2, and has a long repulsive tail. As ε_{cc} increases from kT to $3kT$, the PMF changes from repulsive to attractive, both at contact and $r/D < 1.3$, then becomes more repulsive for $r/D > 1.3$ and has a longer repulsive tail than when $\varepsilon_{cc} = kT$. The trend seen for $\varepsilon_{cc} = 5kT$ and higher is similar to $\varepsilon_{cc} = 3kT$, with the intensity of all features (repulsive and attractive) larger for higher particle−particle attraction strengths. These results suggest that below a critical particle attraction strength (in this case between $\varepsilon_{cc} = 1$ and $3kT$), entropic considerations dominate resulting in a repulsive PMF favoring filler dispersion. Above a threshold attraction strength, enthalpic effects

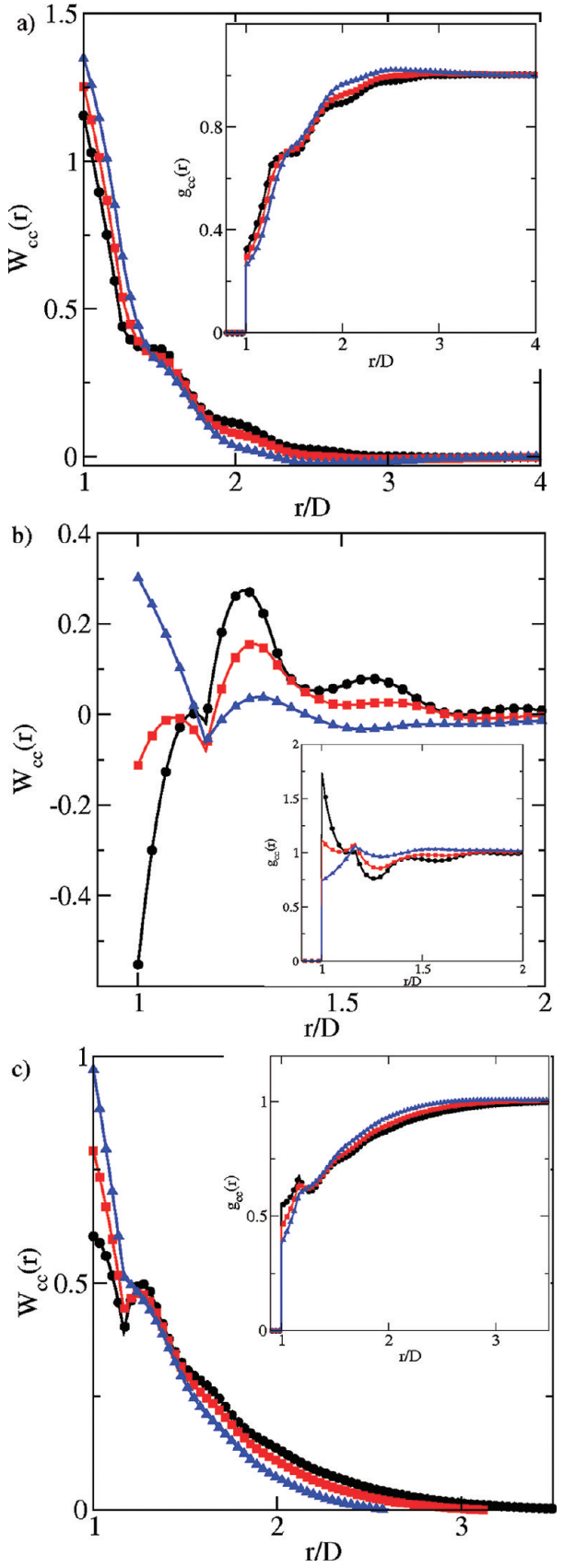

Figure 5. Potential of mean force, $W_{cc}(r)$, and particle−particle pair correlation function, $g_{cc}(r)$, at $\eta = 0.4$, $\phi = 0.2$ (circles), 0.5 (square), and 0.8 (triangle) under athermal conditions for (a) $D/d = 2$ and $N_p = N_m = 8$, (b) $D/d = 3$ and $N_p = N_m = 8$, and (c) $D/d = 3$ and $N_p = N_m = 27$.

dominate and the PMF becomes increasing attractive at contact and favors aggregation. Comparison of the results in Figure 6a to their infinitely dilute analogues (Figure 4a, solid-circles) reveals the $W_{cc}(r)$ are very similar. This suggests that at $\phi = 0.2$ the many body effects are not significant. The corresponding collective structure factors in Figure 6b show an increasing low angle (microphase) peak at $kD \sim 2$ that intensifies as the direct filler attractions increase, suggesting a weak real space ordering.

For the same tether and matrix polymer length, as the nanoparticle size increases to $D/d = 3$ (Figure 6, parts c and d) more filler−filler contacts are expected since a larger fraction of the nanoparticle surface is uncovered. This trend is found in Figure 6c where an attractive PMF at contact and large contact value of $g_{cc}(r)$ are evident (inset of Figure 6c). For constant tether length and $\varepsilon_{cc} = kT$, the most obvious difference is that for $D/d = 3$ the PMF at contact is $-kT$, while for $D/d = 2$ (Figure 6a) it is $+0.4kT$. When $D/d = 3$, as ε_{cc} increases the PMF at contact becomes increasingly attractive, and at intermediate interfiller distances it becomes increasing repulsive, while $S_{cc}(k)$ exhibits an more intense low angle peaks at $kD \sim 2$ and $kD \to 0$. The latter suggests direct filler and matrix-induced depletion attractions result in modest clustering.

If the tether length is increased to $N_p = 27$ (with $N_m = N_p$) keeping the nanoparticle size fixed at $D/d = 3$ (Figure 6e and 6f), the PMF at $\varepsilon_{cc} = kT$ becomes less attractive than the corresponding case where $N_p = N_m = 8$ (Figure 6c). This is because steric shielding by grafted polymers plays a bigger role. As ε_{cc} increases, the main difference between Figure 6c ($D/d = 3$, $N_p = N_m = 8$) and Figure 6e ($D/d = 3$, $N_p = N_m = 27$) is that for longer tethers there are no oscillations in the $W_{cc}(r)$ over the region $1.4 < r/D < 2$ as seen for the shorter tethers. In addition, the repulsive tail in the PMF extends further for the longer tether, which proves that the repulsion beyond contact arises from the grafted chains. The only major difference in the collective filler structure factors (Figure 6d and Figure 6f) is as $kD \to 0$. For the higher tether length there is no effect of ε_{cc} on $S_{cc}(k)$ as $kD \to 0$, while at lower tether length (Figure 6d) increasing ε_{cc} results in an increase of $S_{cc}(k \to 0)$. This supports our previous conjecture that for shorter tether length the increasing value of $S_{cc}(k \to 0)$ is due to the tendency (but not realization) for macrophase separation due to particle−particle attraction and matrix-induced depletion attraction. For longer tether lengths the increased steric hindrance will counter-act this tendency, as evident from the low values of $S_{cc}(k \to 0)$.

Figure 7 plots the PMF, $g_{cc}(r)$, and $S_{cc}(k)$ for the same cases as in Figure 6 but at $\phi = 0.5$. For $D/d = 2$ and $N_p = N_m = 8$ (Figure 7, parts a and b), the PMF is not shown for a kT attraction strength since a converged numerical solution of the PRISM equations could not be obtained. If the $\phi = 0.5$ results are compared to their $\phi = 0.2$ analogues (Figure 6a) some similarities are evident. The PMF at contact for $\varepsilon_{cc} = 3kT$ is slightly less attractive for $\phi = 0.5$ compared to $\phi = 0.2$, perhaps due to increased steric hindrance from grafted polymers. At $\varepsilon_{cc} = 5kT$, the PMF and $g_{cc}(r)$ do not seem to be affected by filler composition. Collective particle−particle structure factors are shown in Figure 7b for ε_{cc} varying from $3kT$ to $9kT$. As ε_{cc} increases the peak at kD∼2 grows, similar to the trend for $\phi = 0.2$ (Figure 6b), but the magnitude of the peaks are higher for $\phi = 0.5$. This is understandable since we expect higher aggregation as the filler volume fraction increases.

For the same tether and matrix polymer length of $N_p = N_m = 8$, as particle size increases to $D/d = 3$ (Figure 7c) we

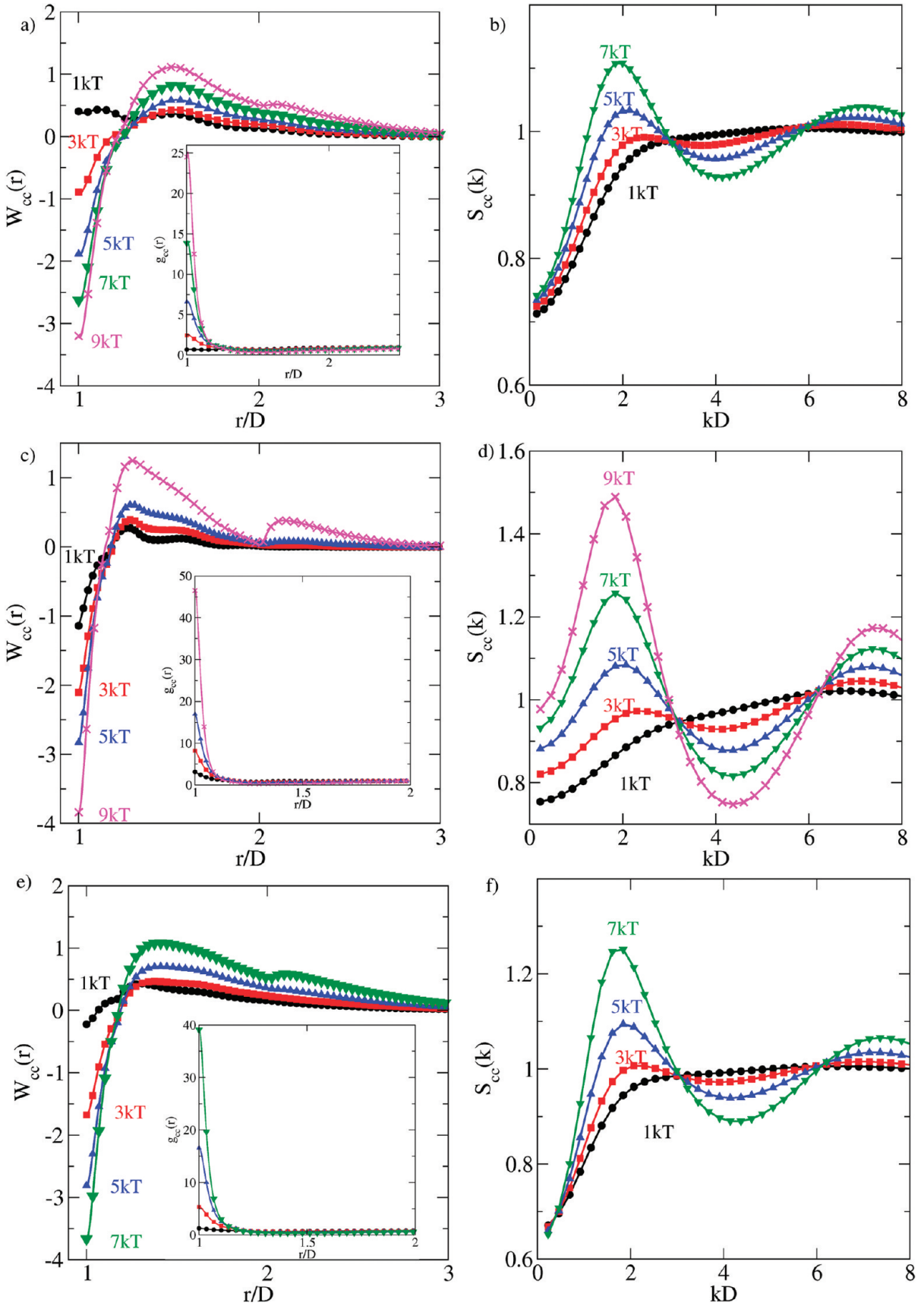

Figure 6. Potential of mean force, $W_{cc}(r)$, particle−particle pair correlation function, $g_{cc}(r)$, and filler collective structure factor, $S_{cc}(k)$, at $\eta = 0.4$, $\phi = 0.2$, at particle−particle attraction strengths of $1kT$ (circle), $3kT$ (square), $5kT$ (upward triangle), $7kT$ (downward triangle), and $9kT$ (cross) for: $D/d = 2$ and $N_p = N_m = 8$ (a and b), $D/d = 3$ and $N_p = N_m = 8$ (c and d), and $D/d = 3$ and $N_p = N_m = 27$ (e and f).

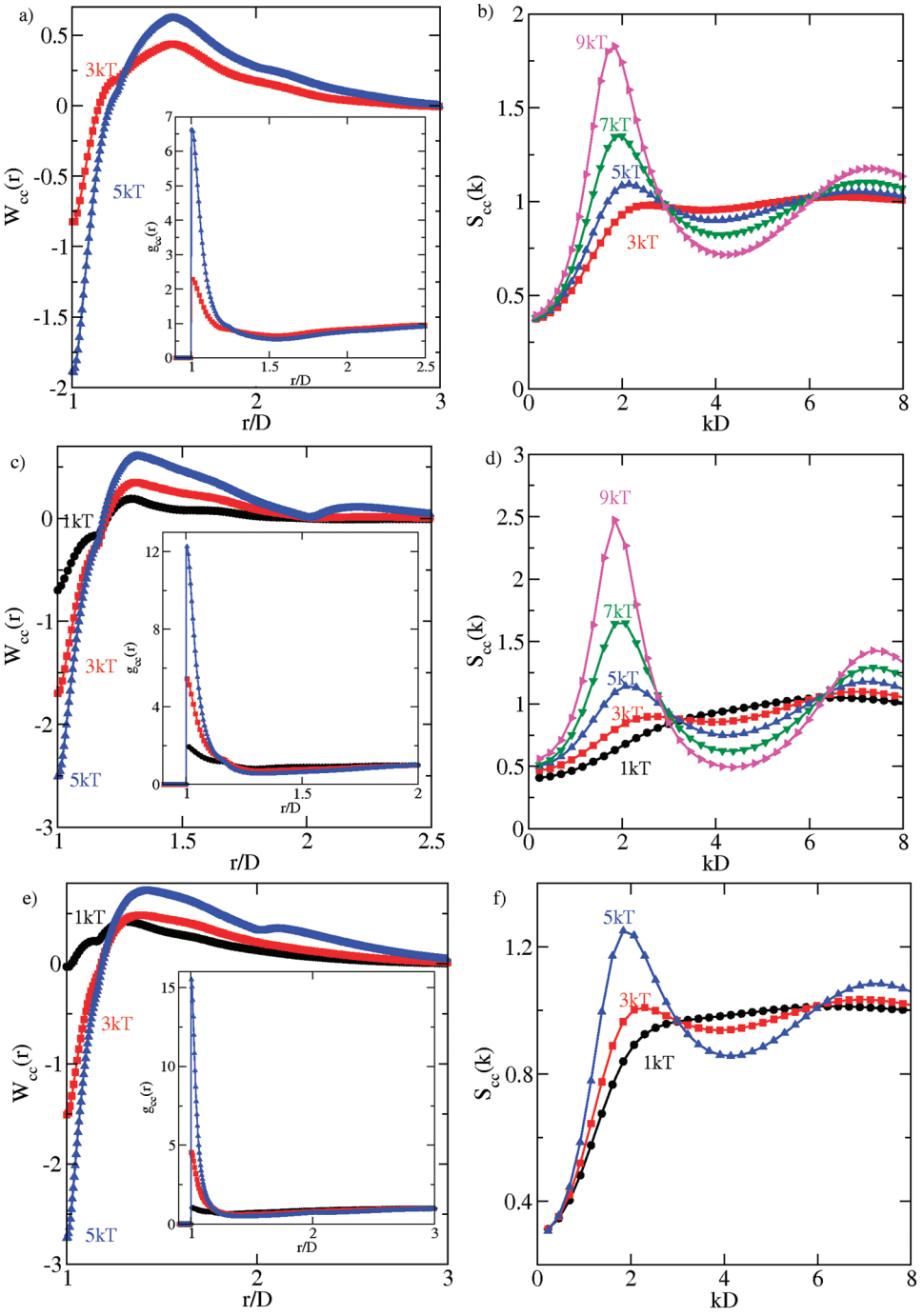

Figure 7. Same as Figure 6 but for $\phi = 0.5$.

find for all filler attraction strengths the trends at $\phi = 0.5$ are similar to those found for $\phi = 0.2$ (Figure 6c), but the PMF at contact attraction is always lower. In addition, the repulsive $W_{cc}(r)$ (correlation hole in $g_{cc}(r)$) for $r/D > 1.2$ is less oscillatory (Figure 6c), the peaks at $kD \sim 2$ in $S_{cc}(k)$ (Figure 7d) are higher, and the effect of filler attraction strength on the $S_{cc}(k = 0)$ diminishes, for $\phi = 0.5$ compared to $\phi = 0.2$. These trends also hold for $D/d = 3$ and $N_p = N_m = 27$ (Figure 7e and 7f), and the differences with filler composition are slightly more dramatic than seen for $D/d = 2$ or 3 at $N_p = N_m = 8$. The primary difference is that the PMF at contact for $\varepsilon_{cc} = kT$ is mostly repulsive for the higher filler composition, while it is attractive for $\phi = 0.2$.

C. Spinodal Microphase Separation. PRISM theory describes correlated and spatially segregated, but globally homogeneous, fluid states. It is not a mean field theory and includes concentration fluctuations on all length scales. Hence, literal spinodal instabilities at nonzero wave vectors (structure factor divergences at k^*) are not predicted.[46,47] However, in extensive prior applications of the theory to diblock[36,46,47] and multiblock[52,53] copolymers, an analysis of small angle scattering profiles was proposed which allows a useful estimate of a microphase separation transition in the sense of an extrapolated spinodal instability. In polymer mean field theories and experimental scattering analyses the quantity $1/S_{cc}(k^*)$ is taken as the order parameter which would vanish at a literal spinodal instability.[54,55]

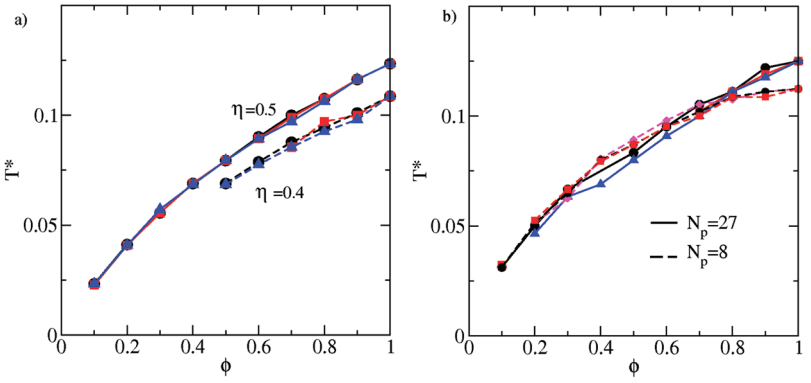

Figure 8. Microphase spinodal reduced temperature (in units of ε_{cc}), T^*, as a function of composition, ϕ, for (a) $D/d = 2$, $N_p = 8$, $N_m = 1$ (circle), 8 (square), and 50 (triangle) at $\eta = 0.5$ (solid) and $\eta = 0.4$ (dashed) and (b) $D/d = 3$, $N_p = 8$ (dashed) and $N_p = 27$ (solid) at $\eta = 0.4$ for varying N_m, $N_m = 1$ (circle), 8 (square) or 25 (diamond), and 50 (triangle).

We estimate the spinodal curve via linear extrapolation of $1/S_{cc}(k^*)$ as a function of the inverse dimensionless temperature, $1/T^* = \varepsilon_{cc}/kT$. When applied to melts of single-tethered particles,[32] the resulting microphase spinodal curve was shown to be in good agreement with the order−disorder boundary obtained from simulations by Iacovella et al.[29] This prior work motivates an analogous analysis of the present tethered nanoparticle PNC.

Figure 8a presents the microphase spinodal reduced temperature, T^*, as a function of composition, ϕ, for $D/d = 2$ with tether length $N_p = 8$ and varying matrix polymer length for $\eta = 0.5$ (solid) and $\eta = 0.4$ (dashed). The microphase spinodal curves display a dilution-like behavior corresponding to a *monotonic decrease* of T^* as fillers are replaced by matrix homopolymers; note, however, the form of the spinodal curve is not linear as would be predicted by a naïve mean field dilution idea. Overall, the trends are in contrast with the complex combination of depletion (homopolymer-mediated increase of T^*) and dilution behavior found for lightly tethered (1 or 2) nanoparticles.[35] For the six tethered particles in Figure 8a the microphase spinodal curves overlap at different matrix polymer lengths. When $D/d = 2$, the tethered chains frustrate thermally driven ordering because they strongly shield the nanoparticle surface. Thus, the matrix polymer induced depletion interactions play a minor role. As the total fluid packing fraction is lowered from 0.5 to 0.4, the spinodal temperature decreases as expected.

Figure 8b presents the microphase spinodal phase diagram for $D/d = 3$ and tether length $N_p = 8$ (dashed) and $N_p = 27$ (solid) at varying N_m and total fluid packing fraction $\eta = 0.4$. Unlike the $D/d = 3$ lightly tethered nanoparticles with one or two polymer tethers,[34] the effect of tether length on the microphase spinodal temperature is only minor with six tethers, detectable only at higher filler compositions. If one compares the spinodals for $D/d = 3$ with tether length $N_p = 8$ (dashed) with the corresponding curves in Figure 8a ($D/d = 2, \eta = 0.4, N_p = 8$), it is clear that a pure dilution-like behavior is not predicted for the larger nanoparticles; rather, as the filler composition decreases a mild depletion-like behavior is also present.

V. Summary and Discussion

We have applied PRISM theory to study the effective interactions, local packing, and phase behavior of spherical nanoparticles with six tethered chains dissolved in a homopolymer matrix under dense melt conditions. Only particle−particle interactions are attractive. Such modestly grafted fillers can experience competing direct interparticle attractions and matrix-mediated effective interactions that are sensitive to filler diameter and the relative and absolute values of tether and matrix degrees of polymerization. This is the physical origin of their complex and tunable behavior. Moreover, the spatial organization of the fillers depends strongly on mixture composition, with nonadditive many body effects often of high importance.

Calculations of the filler potential of mean force, $W_{cc}(r)$, pair correlation function, $g_{cc}(r)$, and collective structure factor, $S_{cc}(k)$, for both athermal entropic conditions and in the presence of filler attractions, at varying filler concentrations, have been presented. Under infinitely dilute athermal conditions, how much of the nanoparticle surface is effectively covered by the grafted chains that sterically shield the direct internanoparticle attraction dictates if the fillers disperse or aggregate, in agreement with recent molecular dynamics results.[34] A critical parameter is the ratio of tether to nanoparticle volume. If this parameter is greater than or equal to unity (e.g., $D/d = 2$ and $N_p = 8$ or $D/d = 3$ and $N_p = 27$), the nanoparticle surface is effectively shielded from close approach to another nanoparticle surface, and the fillers are well dispersed. As the nanoparticle core diameter increases at fixed number and length of tether chains (ratio of tether to particle volume less than unity) the PMF at contact changes from repulsive to attractive since the grafted chains no longer efficiently cover the filler surface.

The six-tethered nanoparticles of $D/d = 2$ (core diameter ~2 nm) have a grafting density of 0.48 chains/nm^2. Thus, increasing matrix length for this system results in a PMF that is more attractive at contact. Such behavior is analogous to the well-known decreased wettability of brush layers as the matrix chain length increases. Since the nanoparticles of core diameter greater than ~3 nm are not densely grafted, the effect of matrix length on the PMF is different and not purely repulsive. For all matrix lengths, upon increasing the grafted polymer length the filler PMF at contact can be switched from attractive to repulsive.

At nonzero filler concentrations and in the presence of direct interparticle attractions, for grafted nanofillers with a core volume that matches the tether volume there exists a critical attraction strength below which the entropic forces dominate resulting in filler dispersion. Above a threshold attraction strength, enthalpic effects dominate and the PMF becomes increasing attractive at contact and favors filler aggregation. The collective particle structure factors show an increasing low angle (microphase) peak that intensifies as the direct filler attractions increase, suggesting a weak real space ordering of the nanoparticles. For the same tether and matrix polymer length, as the nanoparticle size increases less of the filler core is shielded. As a consequence, the PMF at contact becomes increasingly attractive, and $S_{cc}(k)$ exhibits a more intense low angle peak at $kD \sim 2$ and as $kD \rightarrow 0$ with increasing particle attraction.

These trends suggest direct filler and matrix-induced depletion attractions result in nanoparticle clustering.

An extrapolated microphase spinodal phase diagram was determined based on the low angle peak of the nanoparticle collective structure factor. Although the spatial symmetry of any mesoscale crystalline order cannot be deduced, such a calculation does provide insight concerning when the homogeneous fluid phase becomes unstable to microphase ordering. For the six-tethered fillers a dilution-like behavior is found, unlike the phase boundaries for more lightly grafted nanoparticles which exhibit a subtle competition between dilution and depletion effects.[35] For smaller particles ($D/d = 2$), with tether volume matching the filler core volume, the microphase spinodal boundaries exhibit a purely dilution-like behavior, and superimpose at different matrix polymer lengths. For the same tether length and larger particles, a mild depletion-like behavior is also present as filler concentration increases.

We note that ignoring the nonideal conformational effects, although a reasonable first approximation at high melt-like volume fractions in the absence of all matrix polymer and tether polymer attractive interactions, could potentially bias the predicted local structure in these systems. Future work based on a fully self-consistent version of PRISM theory can potentially address this issue. The prediction of true order−disorder phase transitions requires the development of a molecular-scale density functional approach for grafted nanoparticle mixtures which likely will require the homogeneous phase correlations predicted by PRISM theory as input. Finally, our integral equation approach is not only applicable to spherical tethered particles in a homopolymer matrix, but can also treat physical and chemical heterogeneities of nanoparticles (e.g., nonspherical fillers) and/or matrix (e.g., blends, block copolymers).

Acknowledgment. This work was supported by the Division of Materials Sciences and Engineering, U.S. Department of Energy under contract with UT-Battelle, LLC, via Oak Ridge National Laboratory. Helpful and stimulating discussions with Professor Sanat Kumar are gratefully acknowledged.

References and Notes

(1) Krishnamoorti, R.; Vaia, R. A. *J. Polym. Sci., Part B: Polym. Phys.* **2007**, *45*, 3252–3256.
(2) Vaia, R. A.; Maguire, J. F. *Chem. Mater.* **2007**, *19*, 2736–2751.
(3) Winey, K. I.; Vaia, R. A. *MRS Bull.* **2007**, *32*, 314–319.
(4) Akcora, P.; Liu, H.; Kumar, S. K.; J., M.; Li, Y.; Benicewicz, B. C.; Schadler, L. S.; Acehan, D.; Panagiotopoulos, A. Z.; Pryamitsyn, V.; Ganesan, V.; Ilavsky, J.; Thiyagarajan, P.; Colby, R. H.; Douglas, J. F. *Nat. Mater.* **2009**, *8*, 354–359.
(5) Barbier, D.; Brown, D.; Grillet, A. C.; Neyertz, S. *Macromolecules* **2004**, *37*, 4695–4710.
(6) Bhattacharjee, R. R.; Das, A. K.; Haldar, D.; Si, S.; Banerjee, A.; Mandal, T. K. *J. Nanosci. Nanotechnol.* **2005**, *5*, 1141–1147.
(7) Corbierre, M. K.; Cameron, N. S.; Sutton, M.; Laaziri, K.; Lennox, R. B. *Langmuir* **2005**, *21*, 6063–6072.
(8) Glogowski, E.; Tangirala, R.; Russell, T. P.; Emrick, T. *J. Polym. Sci., Part A: Polym. Chem.* **2006**, *44*, 5076–5086.
(9) Harton, S. E.; Kumar, S. K. *J. Polym. Sci., Part B: Polym. Phys.* **2008**, *46*, 351–358.
(10) Kim, B. J.; Fredrickson, G. H.; Kramer, E. J. *Macromolecules* **2008**, *41*, 436–447.
(11) Krishnamoorti, R. *MRS Bull.* **2007**, *32*, 341–347.
(12) Marla, K. T.; Meredith, J. C. *J. Chem. Theory Comput.* **2006**, *2*, 1624–1631.
(13) Reister, E.; Fredrickson, G. H. *J. Chem. Phys.* **2005**, *123*, 214903.
(14) Warren, S. C.; Disalvo, F. J.; Wiesner, U. *Nat. Mater.* **2007**, *6*, 248–248.
(15) Tsubokawa, N. *Polym. J.* **2007**, *39*, 983–1000.
(16) Lan, Q.; Francis, L. F.; Bates, F. S. *J. Polym. Sci., Part B: Polym. Phys.* **2007**, *45*, 2284–2299.
(17) Goel, V.; Chatterjee, T.; Bombalski, L.; Yurekli, K.; Matyjaszewski, K.; Krishnamoorti, R. *J. Polym. Sci., Part B: Polym. Phys.* **2006**, *44*, 2014–2023.
(18) Jones, R. A. L.; Richards, R. W., *Polymers at surfaces and interfaces*; Cambridge University Press: Cambridge, U.K., 1999.
(19) Currie, E. P. K.; Norde, W.; Stuart, M. A. C. *Adv. Colloid Interface Sci.* **2003**, *100*, 205–265.
(20) Westenhoff, S.; Kotov, N. A. *J. Am. Chem. Soc.* **2002**, *124*, 2448–2449.
(21) Song, T.; Dai, S.; Tam, K. C.; Lee, S. Y.; Goh, S. H. *Polymer* **2003**, *44*, 2529–2536.
(22) Song, T.; Dai, S.; Tam, K. C.; Lee, S. Y.; Goh, S. H. *Langmuir* **2003**, *19*, 4798–4803.
(23) Li, B.; Li, C. Y. *J. Am. Chem. Soc.* **2007**, *129*, 12–13.
(24) Kawauchi, T.; Kumaki, J.; Yashima, E. *J. Am. Chem. Soc.* **2005**, *127*, 9950–9951.
(25) Chan, E. R.; Ho, L. C.; Glotzer, S. C. *J. Chem. Phys.* **2006**, *125*, 064905.
(26) Chan, E. R.; Zhang, X.; Lee, C. Y.; Neurock, M.; Glotzer, S. C. *Macromolecules* **2005**, *38*, 6168–6180.
(27) Glotzer, S. C.; Horsch, M. A.; Iacovella, C. R.; Zhang, Z. L.; Chan, E. R.; Zhang, X. *Curr. Opin. Colloid Interface Sci.* **2005**, *10*, 287–295.
(28) Horsch, M. A.; Zhang, Z. L.; Glotzer, S. C. *Phys. Rev. Lett.* **2005**, *95*, 056105.
(29) Iacovella, C. R.; Keys, A. S.; Horsch, M. A.; Glotzer, S. C. *Phys. Rev. E.* **2007**, *75*, 040801.
(30) Iacovella, C. R.; Horsch, M. A.; Zhang, Z.; Glotzer, S. C. *Langmuir* **2005**, *21*, 9488–9494.
(31) Lee, J. Y.; Balazs, A. C.; Thompson, R. B.; Hill, R. M. *Macromolecules* **2004**, *37*, 3536–3539.
(32) Jayaraman, A.; Schweizer, K. S. *J. Chem. Phys.* **2008**, *128*, 164904.
(33) Jayaraman, A.; Schweizer, K. S. *Langmuir* **2008**, *24*, 11119–11130.
(34) Smith, G. D.; Bedrov, D. *Langmuir* **2009**; published online.
(35) Jayaraman, A.; Schweizer, K. S. *Macromolecules* **2008**, *41*, 9430–9438.
(36) Schweizer, K. S.; Curro, J. G. *Adv. Chem. Phys.* **1997**, *98*, 1–142.
(37) Curro, J. G.; Schweizer, K. S.; Grest, G. S.; Kremer, K. *J. Chem. Phys.* **1989**, *91*, 1357–1364.
(38) Grest, G. S.; Kremer, K. *Phys. Rev. A* **1986**, *33*, 3628–3631.
(39) Henderson, D.; Duh, D. M.; Chu, X. L.; Wasan, D. *J. Colloid Interface Sci.* **1997**, *185*, 265–268.
(40) Hooper, J. B.; Schweizer, K. S.; Desai, T. G.; Koshy, R.; Keblinski, P. *J. Chem. Phys.* **2004**, *121*, 6986–6997.
(41) Hooper, J. B.; Schweizer, K. S. *Macromolecules* **2005**, *38*, 8858–8869.
(42) Hooper, J. B.; Schweizer, K. S. *Macromolecules* **2006**, *39*, 5133–5142.
(43) Hall, L. M.; Schweizer, K. S. *J. Chem. Phys.* **2008**, *128*, 234901.
(44) Chandler, D.; Andersen, H. C. *J. Chem. Phys.* **1972**, *57*, 1930.
(45) Schweizer, K. S.; Curro, J. G. *Adv. Polym. Sci.* **1994**, *116*, 319–377.
(46) David, E. F.; Schweizer, K. S. *J. Chem. Phys.* **1994**, *100*, 7767–7783.
(47) David, E. F.; Schweizer, K. S. *Macromolecules* **1997**, *30*, 5118–5132.
(48) Heine, D. R.; Grest, G. S.; Curro, J. G. *Adv. Comp. Simul. Approaches Soft Matter Sci. I* **2005**, *173*, 209–249.
(49) Hindmarsh, A. C.; Brown, P. N.; Grant, K. E.; Lee, S. L.; Serban, R.; Shumaker, D. E.; Woodward, C. S. *ACM Trans. Math. Software* **2005**, *31*, 363–396.
(50) Starr, F. W.; Douglas, J. F.; Glotzer, S. C. *J. Chem. Phys.* **2003**, *119*, 1777–1788.
(51) Striolo, A.; Egorov, S. A. *J. Chem. Phys.* **2007**, *126*, 014902.
(52) Kolbet, K. A.; Schweizer, K. S. *Macromolecules* **2000**, *33*, 1443–1458.
(53) Kolbet, K. A.; Schweizer, K. S. *Macromolecules* **2000**, *33*, 1425–1442.
(54) Bates, F. S.; Fredrickson, G. H. *Annu. Rev. Phys. Chem.* **1990**, *41*, 525–557.
(55) Leibler, L. *Macromolecules* **1980**, *13*, 1602–1617.